Department of Energy (DOE) - Office of Energy Efficiency and Renewable Energy (EERE)

Solid-State Lighting Advanced Technology R&D - 2017
Funding Opportunity Announcement (FOA) Number: DE-FOA-0001613
CFDA Number: 81.086

Research Performance Final Report

Grant #DE-EE0008205

Georgia Tech Research Corporation (GTRC)
Mr. Christopher D'Urbano
505 10th Street, NW
Atlanta, GA 30332-0420
Christopher.Durbano@osp.gatech.edu; Tel: 404 385-0866
Type: Cooperative agreement

Stable White Organic Light-emitting Diodes Enabled by New Materials with Reduced Excited State Lifetime

PI: Bernard Kippelen

DUNS: 09-739-4084

Date: November 26, 2019
Period covered by the report: October 1, 2017 – September 30, 2019

1. Project Overview

***Project Goals and Objectives*.** The Georgia Institute of Technology assembled a multidisciplinary team with complementary expertise in the areas of multi-level molecular simulations (Brédas), chemical synthesis and material characterization (Marder), and device physics and engineering (Kippelen). The team engaged in a two-year integrated theoretical and experimental program to develop blue-emissive layers that can yield simultaneously near 100% internal quantum efficiency (IQE) *and* short excited-state lifetimes to overcome the existing efficiency vs. stability tradeoff displayed by blue-emitting OLEDs and by WOLEDs, and to demonstrate stable WOLEDs that fulfill or exceed the 2020 target metrics (RDP 2016 section C.1.2) ahead of schedule.

To achieve the overall goal, our team set three main objectives:

1) Develop ambipolar hosts with a wide optical bandgap (E_{opt} > 2.8 eV) and an energy difference between their singlet and triplet excited states sufficiently small (ΔE_{ST} < 0.1 eV) for efficient thermally activated reverse intersystem crossing (TA-RISC) at room temperature.
2) Develop blue OLEDs that achieve PE values larger than 50 lm/W with low efficiency roll-off (ca. 15%) through the use of emissive layers comprising wide bandgap low-ΔE_{ST} ambipolar hosts and conventional state-of-the art fluorescent guest emitters.
3) Develop WOLEDs that display power efficacy (PE) values > 50 lm/W, color rendering index (CRI) values > 90 and lumen maintenance (L_{70}) larger than 50,000 h from an initial light output of 10,000 lm/m2.

2. Technical report

Through this program, novel blue-emitting layers were developed based on wide-bandgap ambipolar hosts, having a low energy difference between singlet and triplet excited states (ΔE_{ST}). Compounds having a small ΔE_{ST} can overcome the non-radiative loss of triplet excitons seeing in fluorescent emitters through efficient thermally activated reverse intersystem crossing (TA-RISC) at room temperature, giving rise to thermally activated delayed fluorescence (TADF). When this class of materials are used as emitters, so-called TADF emitters can led to internal quantum efficiency (IQE) values approaching 100% and fluorescent (TADF) OLEDs with performance (efficiency and lifetime) characteristics that are comparable to those displayed by phosphorescent OLEDs. However, the triplet excited states that give rise to TADF have lifetimes that are comparable to those found in some phosphorescent emitters, on the order of microseconds; consequently, blue-emitting TADF emitters can also suffer from limited stability.

Here, we used compounds displaying TADF as host in blue-emitting layers, because synthetic chemistry approaches to design TADF emitters also lead to bipolar transport characteristics. However, key differences in the emission transition dipoles (μ_{em}) and quantum yield of emission (Φ_{em}) are required for compounds to act effectively as host or emitters. For emitters, μ_{em} and Φ_{em} need to be maximized to ensure optimum conversion of excitons to photons, although this is challenging because strategies to reduce ΔE_{ST} typically require limited donor (D)/acceptor (A) wavefunction overlap. In a host, the requirements on μ_{em} and Φ_{em} are considerably relaxed; although the rate of host-to-guest Förster resonance energy transfer (FRET) still depends on μ_{em}, it can, with properly chosen host (energy donor) emission spectra, guest (energy acceptor)

absorption spectra, and appropriate concentrations, occur much more rapidly than emission from the host. Furthermore, since the rate of TA-RISC is thermally activated with barrier height ΔE_{ST}, hosts with ΔE_{ST} ca. zero are also expected to show short excited-state lifetimes (τ).

Reducing excited state lifetimes is important because long-lived excited states are believed to lead to the formation of non-radiative recombination centers, luminescence quenchers, and deep charge traps which eventually limit the efficiency at high luminance and stability of blue OLEDs.

In this program, we investigated two general approaches involving the development of wide-bandgap ambipolar hosts with a low ΔE_{ST}. Ambipolar host achieved by *intermolecular through-space* D:A interactions and by *intra*molecular *through-bond* interactions between covalently linked D and A segments. Novel hosts were incorporated in to blue-emissive layers (EML) by combining them with suitable fluorescent guest emitters having high quantum yields of emission (Φ_{em}) to demonstrate blue-emitting OLEDs with high EQE and low roll-off. Finally, we incorporated blue-emitting layers into tandem WOLED architectures.

This report describes the most important results achieved during this program. These results are organized by the tasks performed and integrate synthetic, computational, and device-related work when appropriate.

Task 1.1 Wide-bandgap low-ΔE_{ST} ambipolar D:A intermolecular host

In this task we investigated wide-bandgap low-ΔE_{ST} ambipolar D:A intermolecular host. Work was divided in the following subtasks.

Subtask 1.1.1- Characterization of films of commercially-available D:A molecules: We characterized the formation of D:A exciplex states using commercially available D and A materials. Computational studies were conducted. We met the milestones for this task.

Subtask 1.1.2- Optimization of D:A intermolecular host: After work conducted during budget period 1 we decided not to continue work related to this subtask.

Key Technical Milestone Y1- D:A intermolecular host film with $E_{opt} > 2.7$ eV and $\Delta E_{ST} < 0.3$ eV was demonstrated during year 1.

Key Technical Milestone Y2- D:A intermolecular host film with $E_{opt} > 2.8$ eV and $\Delta E_{ST} < 0.1$ eV was demonstrated during year 1.

Results:

We conducted experimental characterization of the photoluminescent properties of five commercially available, donor (D): acceptor (A) pairs shown in Figure 1.

Co-evaporated films of the five D:A pairs were fabricated on Si-wafer and on UV grade fused silica substrates. The complex refractive index of D, A, and D:A (1:1) films deposited on Si-wafer substrates was derived by fitting the data from spectroscopic ellipsometry measurements acquired by a J.A. Woollam M-2000 ellipsometer and by using the software CompleteEASE™ by J.A. Woollam Co.,Inc.. Refractive index (n) and extinction coefficient (k) were derived by fitting the data using a B-spline model. In all cases, fitted data displayed a mean squared error (MSE) <10. The optical bandgap, E_{op}, defined as the onset of the extinction coefficient, was derived from these measurements on D and A films. In D:A films, the strength of the CT band was too weak to resolve from these measurements. In this case, the onset of the PL emission was used to provide an approximate value to E_{opt}. The photoluminescence (PL) spectra and photoluminescence quantum yield (PLQY) of the D, A, and D:A (1:1) films were also measured.

Acceptor		Donor	
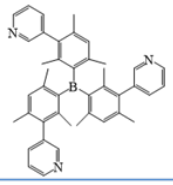	**3TPYMB,** Tris(2,4,6-triMethyl-3-(pyridin-3-yl)phenyl)borane	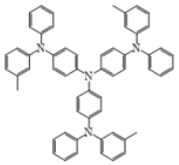	**m-MTDATA,** 4,4′,4′′-tris (3-methylphenylphenylamino) triphenylamine
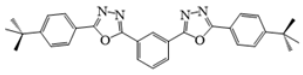	**OXD-7,** 1,3-bis[2-(4-tert-butylphenyl)-1,3,4-oxadiazo-5-yl]-benzene	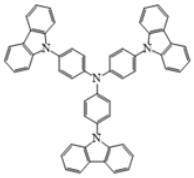	**TCTA,** tris(4-carbazoyl-9-ylphenyl)amine
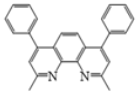	**BCP,** 2,9-dimethyl-4,7-diphenyl-1,10-phenanthroline		**TCTA**
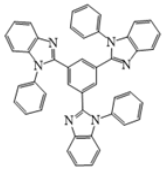	**TPBi,** 2,2′,2″-(1,3,5-benzinetriyl)-tris(1-phenyl-1-H-benzimidazole)		**TCTA**
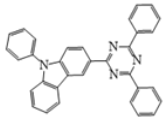	**DPTPCz,** 3-(4,6-diphenyl-1,3,5-triazin-2-yl)-9-phenyl-9H-carbazole		**TCTA**

Figure 1. Chemical structures of donor and acceptor pairs studied.

For PL measurements, UV grade fused silica (ESCO Optics, Inc) slides (12.7 mm Diameter, 1 mm thickness) were loaded into the EvoVac system until it was pumped down to a vacuum level of 1.0 × 10^{-7} Torr. Single layer of neat films or mixed films with a thickness of 50 nm were then deposited on top of the slides with a deposition rate below 1.0 Å/s. The films were then transferred in a nitrogen-filled cylinder to a PL quantum yield spectrometer (Quantaurus-QY C11347, Hamamatsu), where a flow of nitrogen kept bubbling to the sample stage during measurements. Excitation wavelength was 300 nm for all films.

Figure 2 shows a comparison of the complex refractive index and normalized PL measured in films of: (left) 3TPYMB, m-MTDATA and 3TPYMB:m-MTDATA; and (right) TPBi, TCTA and TPBi:TCTA. Similar data sets were produced for the rest of the D:A exciplex systems displayed in Fig. 1. These two material systems also represent the greenest-emitting host (3TPYMB:m-MTDATA) and the bluest-emitting host from the materials selected.

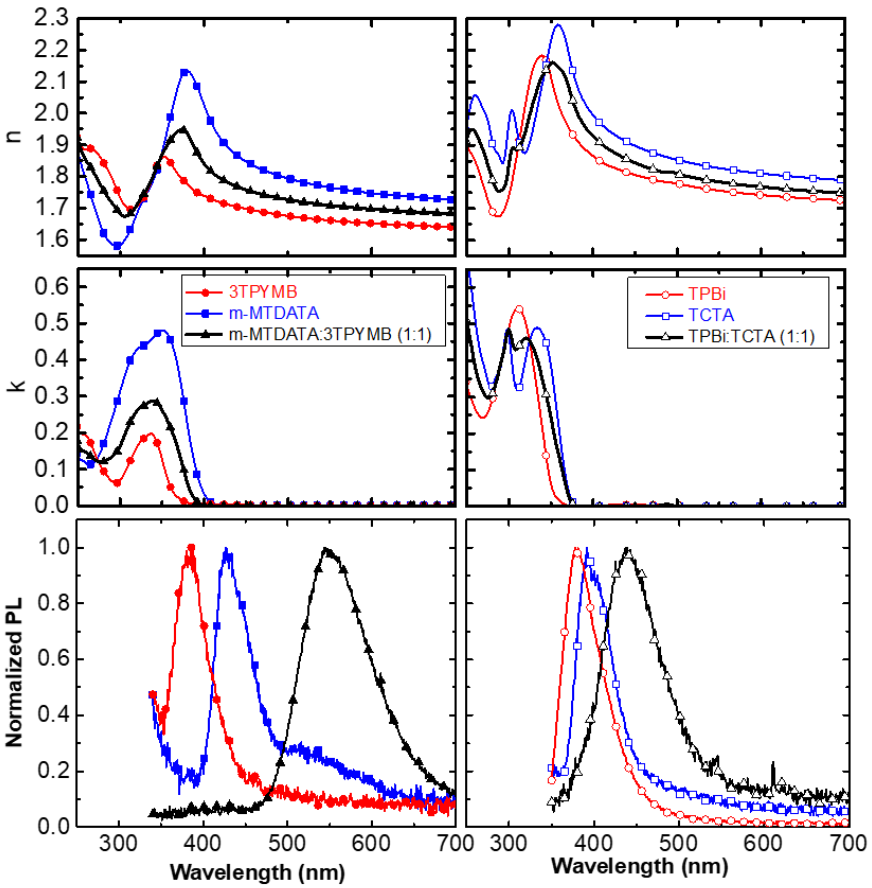

Figure 2. Comparison of complex refractive index and normalized PL in: (left) 3TPYMB, m-MTDATA and 3TPYMB:m-MTDATA; and (right) TPBi, TCTA and TPBi:TCTA.

We computed the distributions of the energies of the lowest charge-transfer (CT) and excitonic states in these blends. As an example of these calculations we present results for the m-MTDATA/3TPYMB blend; where m-MTDATA acts as donor and 3TPYMB acts as acceptor. The blend morphology (see Fig. 3) was obtained by means of molecular dynamics (MD) simulations using all-atom optimized potentials for liquid simulations (OPLS-AA) force field. The MD simulations were performed using a unit cell containing randomly distributed 250 donor molecules and 250 acceptor molecules.

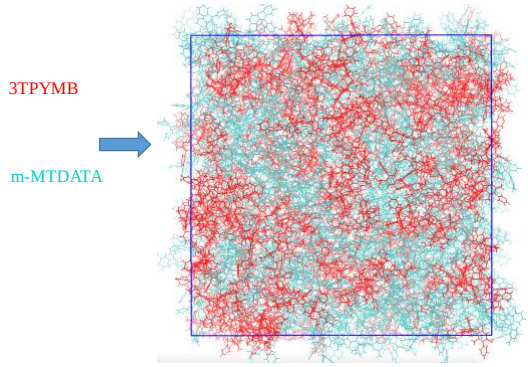

Figure 3. A representative snapshot of m-MTDATA/3TPYMB from MD simulations.

To evaluate the distribution of the CT and excitonic (local excitation, LE) energies, we extracted the coordinates of 1,500 m-MTDATA/3TPYMB complexes from MD-generated morphologies and computed their excited states. Excited-state transition energies were obtained by means of time-dependent density functional theory (TDDFT) calculations based on the Tamm-Dancoff approximation and using the SRSH-ωPBE-D3 hybrid functional (a screened range separated hybrid functional) and the 6-31G(d) basis set. The derived distributions are shown in Figure 4.

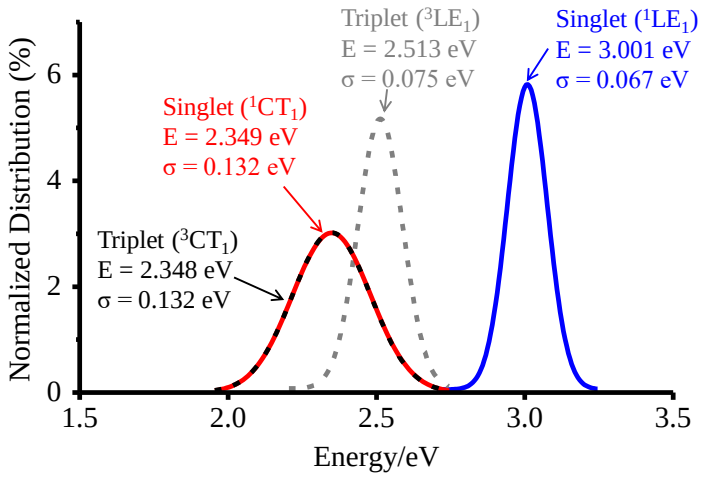

Figure 4. Distribution of singlet and triplet CT and LE energies in m-MTDATA/3TPYMB blend.

Calculated energy values are dependent on the material's dielectric constant. We measured the low frequency/DC dielectric constant of these materials to compare experimental and theoretical results. Figure 5 shows a correlation between the magnitude of the optical bandgap and the calculated ΔE_{ST} values. Calculated ΔE_{ST} values are generally very small and in the range where significant TADF should be observed if the relevant ΔE_{ST} is $\Delta E(^1CT_1 - ^3CT_1)$ instead of $\Delta E(^1CT_1 - ^3LE_1)$, as suggested in the literature. However, the PLQY values were found to be larger for intermolecular systems having smaller $\Delta E(^1CT_1 - ^3CT_1)$ values, which suggests that $\Delta E(^1CT_1 - ^3LE_1)$ may indeed be the relevant metric.

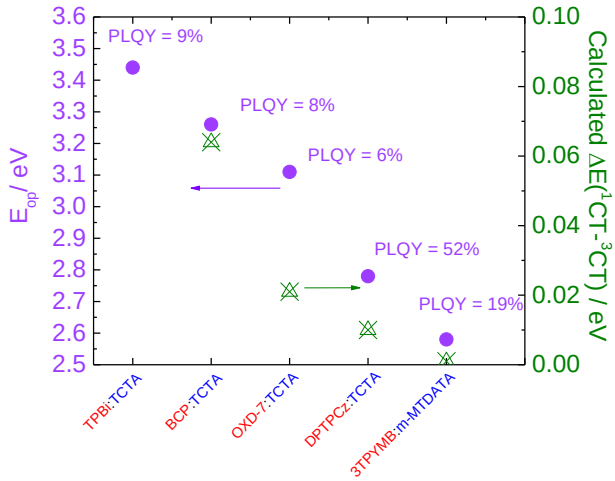

Figure 5. Chemical structures of donor and acceptor pairs studied. Optical bandgap values derived from spectroscopic ellipsometry, photoluminescence quantum yield (PLQY) and estimated ΔE_{ST} derived from theoretical calculations.

Experimental and theoretical studies on the properties of these five D:A pairs resulted in the identification intermolecular hosts meeting the program's metrics. In particular, TPBi:TCTA was identified as the most promising intermolecular host.

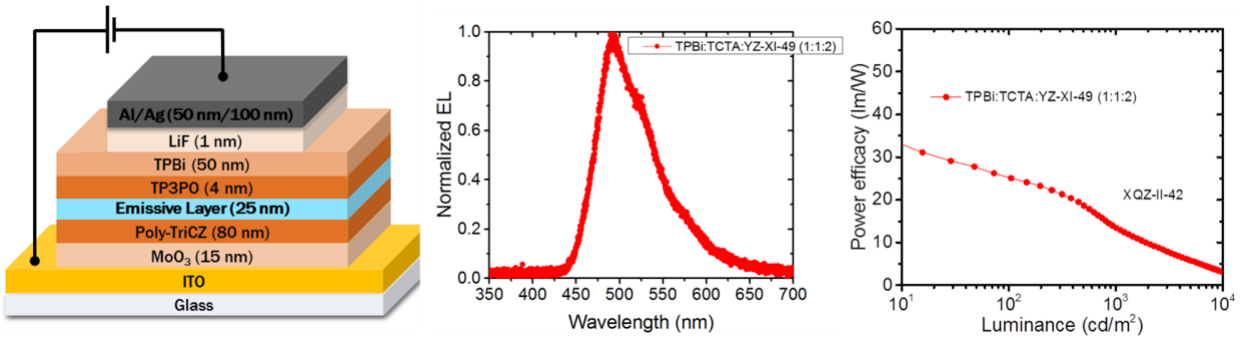

Figure 6. OLED structure (left); Electroluminescent spectra (center); Power efficacy vs. luminance.

Blue-emitting OLEDs were fabricated using TPBi:TCTA as intermolecular host and YZ-V-49 as a TADF emitter, as shown in Figure 6. OLEDs displayed sky-blue emission and an external quantum efficiency (EQE) of ca. 13 % and power efficacy up to 30 lm/W at 10 cd/m2. Despite meeting the material program's metrics, work on Task 1.1 was not continued during year 2 due to the superior performance and ease of fabrication of devices using intramolecular hosts.

Task 1.2 Wide-bandgap low-ΔE_{ST} ambipolar D-A intramolecular hosts

We investigated theoretical and experimental designs and synthesis of ambipolar D-A intramolecular hosts. Work was divided in the following subtasks.

Subtask 1.2.1- Synthesis and characterization of 1-gen hosts: We synthesized and characterized 1-gen hosts based on carbazole donors and phosphine oxide acceptors. We met the milestones for this task.

Subtask 1.2.2- Synthesis and characterization of 2-gen hosts: We synthesized and characterized 2-gen hosts. We calculated molecular properties (DFT) and bulk properties (MD) to guide synthetic efforts for 3-gen D-A intramolecular hosts. We met the milestones for this task.

Subtask 1.2.3- Synthesis and characterization of 3-gen hosts: We synthesized and characterized 3-gen hosts. We calculated molecular properties (DFT) and bulk properties (MD). We met the milestones for this task.

Key Technical Milestone Y1: D-A intramolecular compounds with E_{opt} > 2.7 eV and ΔE_{ST} < 0.3 eV was demonstrated by end of year 1

Key Technical Milestone Y2: D-A intramolecular compounds with E_{opt} > 2.8 eV and ΔE_{ST} < 0.1 eV was demonstrated during year 2

Results:

Many insights into structure-property relations for a variety of D-A classes were developed.

As an example, we investigated the properties of carbazoles in combination with fluorinated aromatic electron-accepting bridging groups. Their photoluminescence was characterized in solution and two groups selected: Group 1 wherein the strength of the donor groups is varied and the electron-accepting bridging group is the same; and Group 2 wherein the number of carbazoles

(*n*) linked to the electron-accepting bridge is varied. Compounds were purified by zone sublimation and films of these materials fabricated and characterized. A summary of the parameters derived from these measurements is presented in Table 1.

Table 1. E_{op} and ΔE_{ST} values for selected intramolecular compounds.

Compound	**E_{op}, eV solution**	**E_{op}, eV film**	**PLQY, % film**	**PL_{peak}, eV / nm film**	**ΔE_{ST} ** meV solution**
Group 1					
YZ-XI-101b/YZ-IX-105	3.22	3.25	54	2.90 / 428	200
YZ-X-7	3.10	-	-	-	100
YZ-XI-105	3.19	3.19	16	2.64 / 470	70
YZ-X-51	2.9	3.05	7	2.61 / 537	-160
Group 2					
YZ-IX-107 (n=2)	3.34	3.33	48	2.97 / 418	380
YZ-X-105b/107a (n=4)	3.28	3.20	33	2.86 / 433	270
YZ-X-105c/107c (n=6)	3.02	3.08	27	2.70 / 460	140
YZ-X-205a (n=8)	2.99	-			-2
YZ-X-205b (n=9)	2.95	-			1

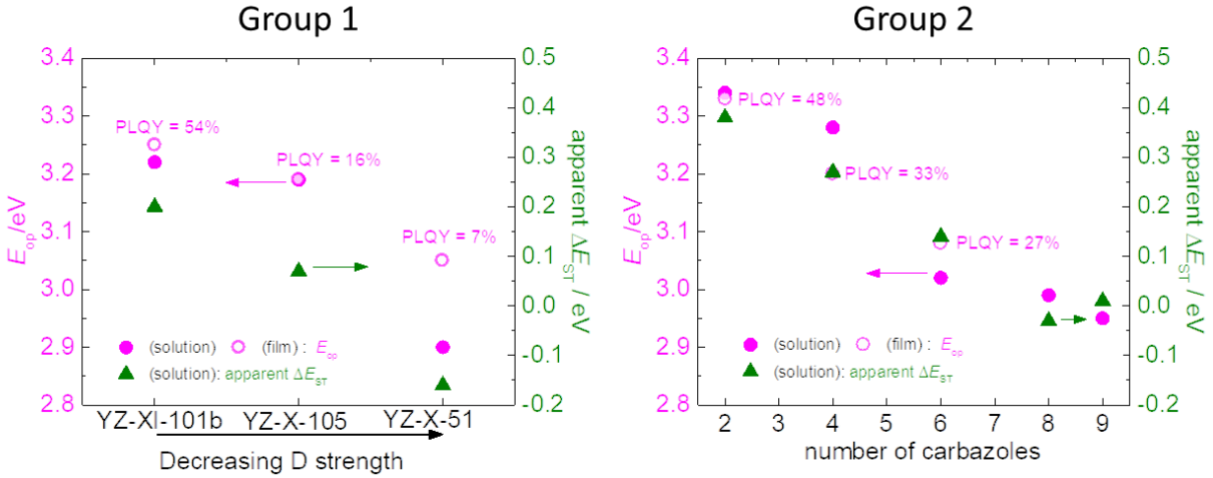

Figure 7. Optical bandgap and apparent ΔE_{ST} measured in solution and in 50 nm-thick films of compounds in Groups 1 and 2.

Table 1 shows a summary of physical parameters derived from PL studies. Figure 7 shows a side to side comparison of the optical bandgap and apparent ΔE_{ST} measured in solutions and films of compounds in Groups 1 and 2. These results reveal that a tradeoff exists between achieving large optical bandgap values and, at the same time, small apparent ΔE_{ST}. However, this tradeoff appears less stringent in compounds from Group 2.

Following these insights learned, we studied carbazole-azaarene molecules; specifically, carbazole-pyrazines, as shown in Figure 8. This group was selected since carbazole-triazines reported in the literature were shown to meet this program's metrics.[1] As Figure 8 shows, it was found that an increase in the number of donors leads to a significant reduction of the ΔE_{ST} values down to ca. 0.150 eV in compounds of type II. These molecules also show wide optical bandgaps

(E_S in the figure) with values up to 3.1 eV. Generally, it was observed that an increased donor strength led to a reduction of ΔE_{ST} values as in Group 1 compounds previously discussed.

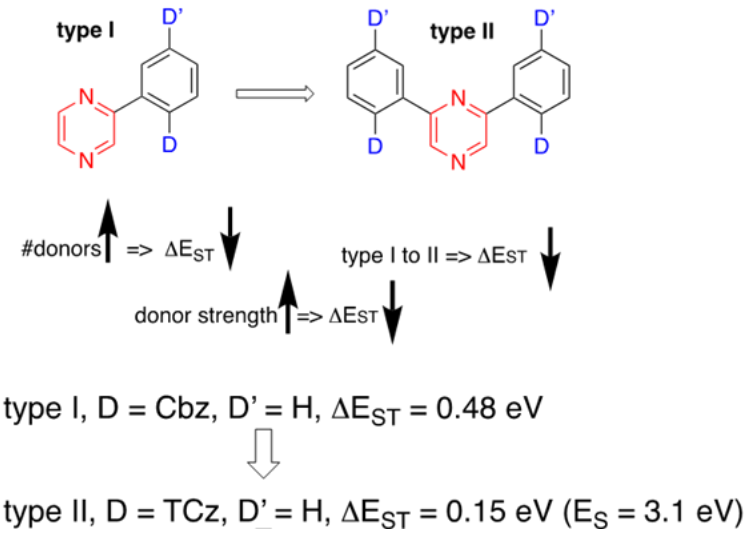

Figure 8. Schematics of type I and type II carbazole-triazines investigated.

An interesting result of these class of compounds was the demonstration that blue-sky-emitting OLEDs with single material emissive layers can yield high EQE values of up to 14% at a luminance of 1,000 cd/m2.[2] Through this program, we found this single-material emissive layer approach to be general, albeit efficiencies where found to be higher for compounds with smaller bandgap values than the ones targeted for this program.[3]

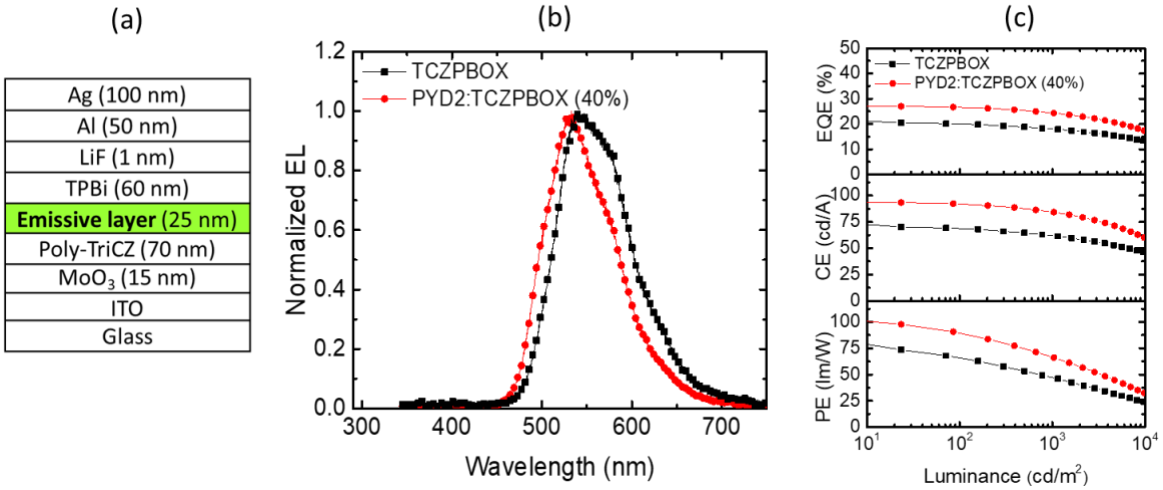

Figure 9. a) OLED structure; b) Electroluminescence spectrum; c) external quantum efficiency (EQE), current efficacy (CE), and power efficacy (PE) vs Luminance.

Figure 9 shows the structure of OLED having a single material (host-free) emissive layer. These yellow-green emitting OLEDs yield a maximum external quantum efficiency (EQE) of 21%, current efficacy (CE) of 73 cd/A, and power efficacy (PE) of 79 lm/W at a luminance of 10 cd/m2. At a high luminance of 10,000 cd/m2, a high EQE of 13% is maintained. A maximum luminance of 120,000 cd/m2 is reached at an applied voltage of 9.8 V. When TCZPBOX was doped in the

host 2,6-di(carbazol-9-yl)-pyridine (PYD2) at 40 wt. %, the device yielded a maximum EQE of 28%, CE of 94 cd/A, and PE of 100 lm/W at 10 cd/m2.3 The high performance of these OLEDs suggests that TADF materials used as host-free EMLs in OLEDs can lead to good charge balance, suggesting effective bipolar transport properties resulting from the donor and acceptor moieties present in the TCZPBOX molecular structure. We believe that this work represents a significant step toward realizing the potential of OLEDs with host-free TADF emitters, which we believe is an attractive route to further simplify the device architecture of OLEDs to be used in display and lighting applications.

To rationalize these results, we conducted theoretical calculations on emissive layers comprising a single compound. Figure 10 shows the results of MD calculations from which we conclude that the emissive layer is in a glassy state at 300 K. The ortho-linkage between the donor and acceptor sub-units of the emitter imposes a twisted structure which favors intramolecular noncovalent interactions; recently it was shown that these types of interactions enhance spin–orbit couplings between the S1 and T1 states, significantly improving the reverse intersystem crossing rates. Importantly, the highly twisted structure of the emitter is found to disfavor intermolecular co-facial π–π stacking configurations. As a result, the emitter S1 and T1 state energies are hardly influenced by interactions among adjacent emitters in the thin film; these excited states are essentially localized on monomers, which leads to only a small probability of formation of intermolecular CT excitations.

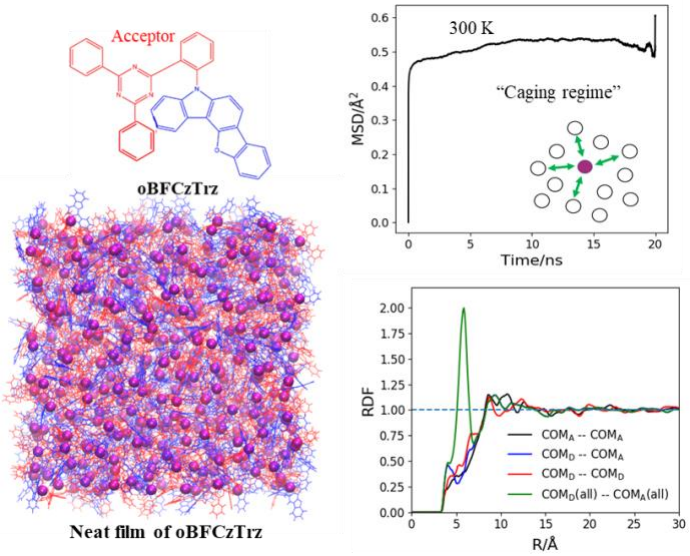

Figure 10. top-left) Chemical structure of oBFCzTrz;. Bottom-left) Illustration of the MD simulation cell containing 400 oBFCzTrz molecules. The donor, acceptor, and center of mass (COM) of each molecule are shown in blue, red, and magenta, respectively. Top right) Mean-square-displacements (MSDs) of the COMs as a function of simulation time at 300 K. Bottom right) Radial distribution functions (RDFs) between COMs of individual oBFCzTrz molecules (shown as magenta balls in bottom left) at 300 K as a function of separation distance (R). Also shows RDFs for COMs of donor (D) and acceptor (A) fragments of the system at 300 and the RDFs between all the donor and acceptor subunits of the system, shown in green.

Consequently, as Figure 11 shows, the electronic structure (natural transition orbitals, NTO) of oBFCzTrz is not significantly altered by intermolecular interactions.4 The excitation energy-transfer calculations confirm that the Förster mechanism is the dominant pathway of energy transfer among oBFCzTrz molecules. The rates of energy transfer are found to be very small,

making exciton–exciton annihilations in the emissive layer unlikely. Combined with the absence of cofacial π–π stacking, this result explains the lack of luminescence quenching in oBFCzTrz neat films.

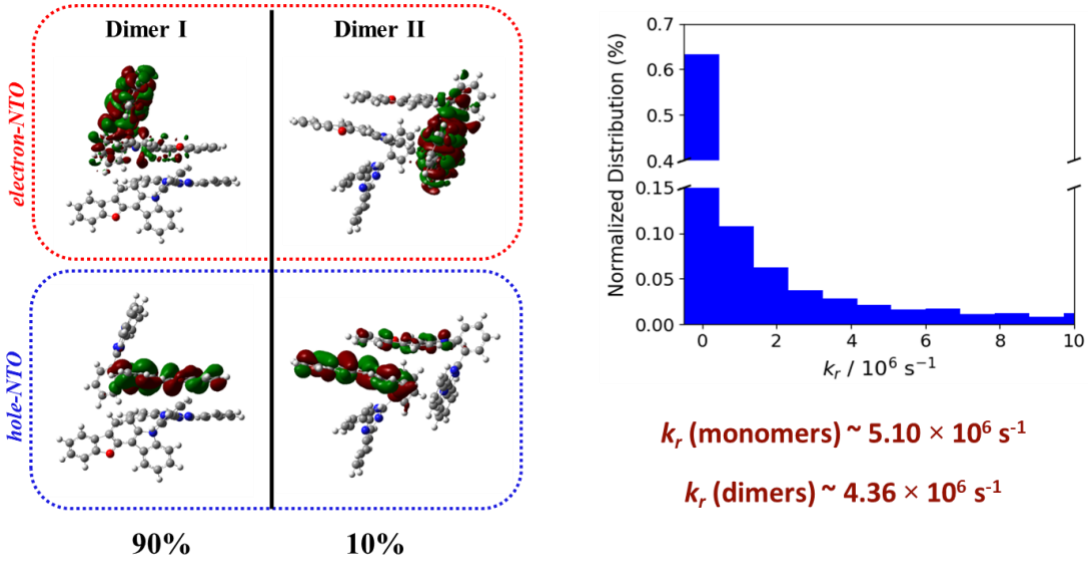

Figure 11. left) Natural transition orbitals for S1 in two representative dimers of oBFCzTrz. Atom color code: C, gray; H, white; N, blue; O, red. Right) Normalized distributions of the radiative decay rates (k_r) for the 1,600 monomers of oBFCzTrz extracted from the MD simulations.

Alternative donors such as p-dimethoxybenzene, were found to be rather weak donors, with some compounds being close to the targeted metrics as shown in Figure 12.

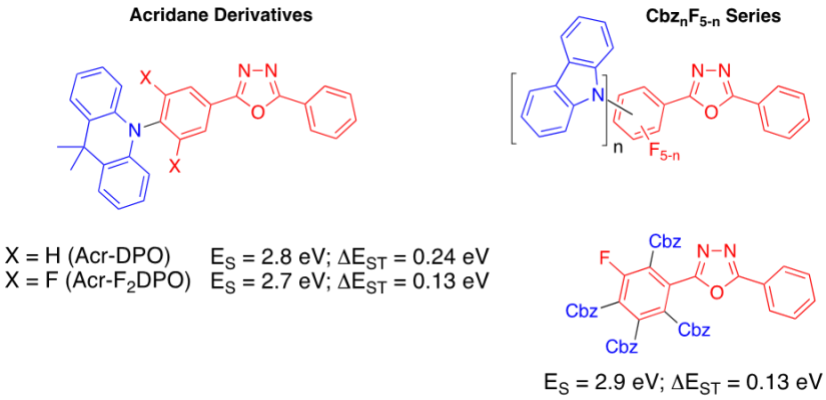

Figure 12. Schematics of diphenyloxadiazole derivatives investigated.

Systematic studies on this class of compounds yielded materials with blue-sky emission. When these compounds where blended with DPEPO, OLEDs with external quantum efficiency (EQE) values up to 24% at a luminance of 10 cd/m2 but also displayed a relatively large EQE roll off, showing EQE values ca 9% at 1,000 cd/m2.5, 6 Although the emission of these compound lies outside of the region of interest, our work helped elucidate the importance of the regiochemistry of donor and acceptor moieties in TADF compounds, beyond the previously postulated ability of the donor to simply inductively stabilize the LUMO on the acceptor.

Finally, derivatives of carbazole-sulfone molecules where also synthesized and investigated as shown in Figure 13. This class of compounds was found particularly promising since a few of them showed optical gaps (E_S) > 3.0 eV and $|\Delta E_{ST}|$ < 90 meV with moderate PLQY values ca 45%. These compounds where not investigated in device architectures since they were developed at the end of the program.

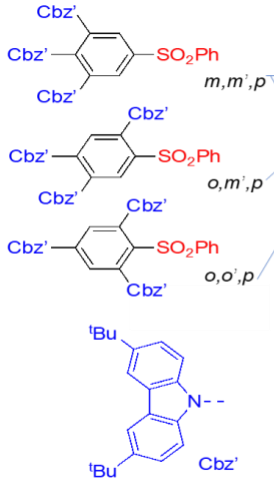

	E_S / eV	ΔE_{ST} / eV	PLQY in air; N_2 / %	PLQY neat film / %
YZ-IX-137	3.1	0.08	37; 92	46
YZ-IX-171	3.1	0.09	19; 56	40*
YX-IX-165	3.0	-0.09	11; 18	47

*85% as 25 wt% blend with DPEPO

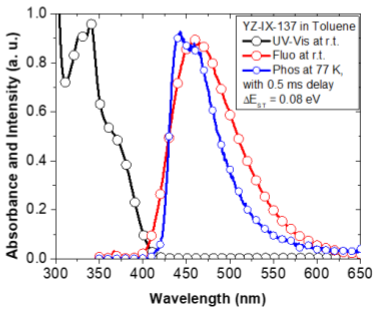

Figure 13. Schematics of carbazole-sulfone derivatives investigated.

Task 2.1 Blue-emitting OLEDs

We identified combinations of blue fluorescent emitters and wide-bandgap low-ΔE_{ST} ambipolar hosts which display efficient Förster resonance energy transfer (FRET) from the host to the guest as well as, inefficient Dexter energy transfer (DET) and evaluated their properties in device structures.

Subtask 2.1.1 Blue EML:

We selected, acquired and purified commercially available guest emitters. We scaled-up previously synthesized D-A intramolecular host 3,5-di(carbazol-9-yl)-1-phenylsulfonylbenzene (mCPSOB). We conducted investigation of Förster resonance energy transfer (FRET) in first-generation blue EML as well as computational studies of packing of selected host/guest systems and the energy transfer processes (FRET and DET) between host and guest emitter. We met partially the milestones for this task.

Subtask 2.1.2 Blue OLEDs:

We fabricated and characterized blue OLEDs, providing validation of the EML selection for WOLED studies and device optimization. We met partially the milestones for this task.

Subtask 2.1.3 Photoluminescence lifetime.

We designed and built a new setup to conduct photoluminescence lifetime studies. We characterized the PL lifetime of various compounds in air and under nitrogen. We met partially the milestones for this task.

Key Technical Milestone Y1: B-OLEDs PE > 40 lm/W; EQE roll-off ca. 20% demonstrated by end of year 1

Key Technical Milestone Y2: Host with Eopt > 2.8 eV and ΔE_{ST} < 0.1 eV with 80% efficient FRET to fluorescent dopant and excited-state lifetime < 1 µs demonstrated during year 2

Key Technical Milestone Y2: B-OLEDs PE > 50 lm/W; EQE roll-off ca. 20% and L70% > 10,000 h at 1,000 cd/m2 not achieved.

Results:

We studied the photoluminescence properties of new derivatives. We incorporated most promising compounds on OLEDs to investigate their electroluminescent properties. We initially used compounds YZ-IX-105 and YZ-X-7 from group 1 and YZ-IX-107 from group 2 as host for TBPe. The best device performance was found in OLEDs having an emissive layer comprising YZ-X-7:TBPe(0.7%), achieving an EQE of ca. 5% at 1,000 cd/m2. These studies suggested an inefficient FRET from the selected hosts to TPBe due to poor spectral overlap. For the first and second generation of intramolecular hosts the highly efficient TADF blue-green emitter YZ-I-49 was used for benchmarking.

Taking advantage of the ambipolar transport properties shown by these types of compounds, we also fabricated OLEDs with so-called single material emissive layers (i.e. host-free). These experiments resulted in devices with relatively low external quantum efficiency with values below 5%. It is believed that unbalanced electron and hole transport led to this poor performance. To test this hypothesis, the intramolecular TADF host was mixed at similar volume ratios with more "conventional" fluorescent hosts such as DPEPO, to improved charge balance and EQE values. These emissive layers are different from conventional guest-host systems, in that the "host" seldom participates in charge transport and recombination, but rather mediates the balance of holes and electrons in the emissive layer. In this way, devices with an emissive layer comprising DPEPO:YZ-X-7 (32 vol.%) achieved EQE values of ca. 10% at a luminance of 400 cd/m2.

With this in mind, we investigated the properties of OLEDs having the emitter YZ-XI-49 and the hosts YZ-VI-11 (mCSOP having a ΔE_{ST} of ca. 360 meV) and YZ-XI-10 (having a ΔE_{ST} of ca. 610 meV). Figure 14 shows the device performance of OLEDs having different volume ratios between YZ-VI-11 and YZ-XI-49. Devices with an EML of YZ-VI-11:YZ-XI-49 at 2.8:1 volume ratio yields OLEDs with a maximum power efficacy of ca. 50 lm/W and EQE roll-off smaller than ca. 20% at 1,000 cd/m2, meeting the performance metric set for year 1.

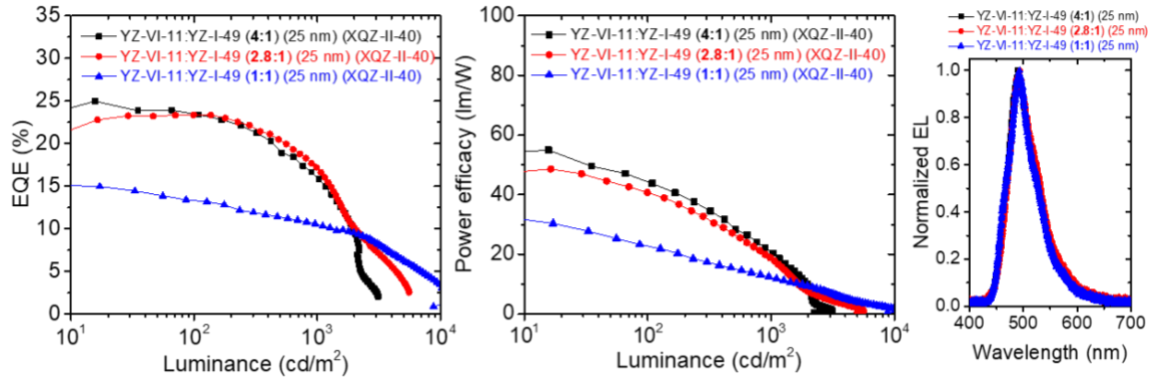

Figure 14. Power efficacy, EQE and EL spectra of OLEDs having EMLs comprising YZ-VI-11 and YZ-XI-49 co-deposited at different volume ratios.

During the second year, most of our work concentrated on screening novel host with the potential to yield efficient FRET into the fluorescent compound TBPe. TBPe was selected because it is a model blue-emitting compound that is used to benchmark blue OLED performance and lifetime. We identified intramolecular hosts that combined a small ΔE_{ST} with an efficient FRET, in particular, we selected 4CzDPO (a.k.a. YZ-V-79, E_{opt} ca. 3.10 eV in solution and ΔE_{ST} ca. 20 meV). Photoluminescence studies showed that the PLQY of 4CzDPO increased from 17% in neat films of the pristine material to up to 88% in films with a composition of 4CzDPO:TBPe (96:4). The photoluminescence spectra of films of 4DCzPO, TBPe and the blend 4CzDPO:TBPe are shown in Figure 15(a). In addition, a significant reduction of the delayed fluorescence lifetime (exciton lifetime), was clearly observed in this system, as shown in Figure 15(b), resulting in an excited-state lifetime ca. 2 µs, very close to fulfilling the target metric of 1 µs. A similar derivative to 4CzDPO, YZ-V-89 (PLQY 9%, E_{opt} ca. 3.06 eV in powder and ΔE_{ST} ca. -10 meV), also showed FRET to TBPe, with PLQY values of 73% in the blend YZ-V-89:TBPe (97:3).

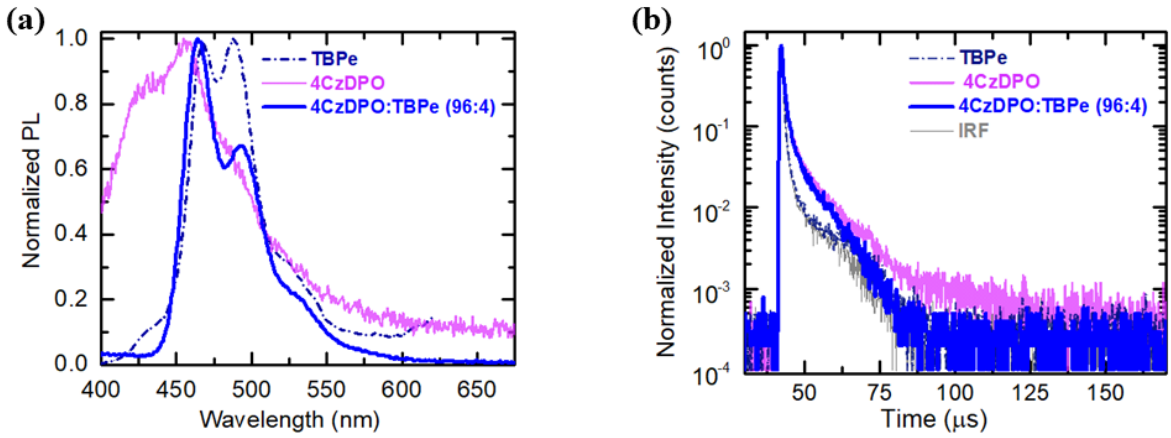

Figure 15. (a) Comparison of normalized photoluminescence of thin films of TBPe, 4CzDPO and 4CzDPO:TBPe. (b) Comparison of the instrument response function (IRF) and the time-dependent photoluminescence in the same thin films shown in (a).

We studied EML layers comprising: TPBi:TCTA:TBPe (48:48:2 vol.%); YZ-XI-39:TBPe(97:3 vol.%); YZ-V-89:TBPe (97:3 & 94:6 vol.%); 4CzDPO:TPBe(97:3 vol.%); The results of the

device characterization are shown in Figure 16. In all cases, all these EML layers showed good rectification characteristics with sample 4CzDPO:TPBe(97:3 vol.%) yielding the highest current density in forward bias as well as the highest maximum luminescence with a values of 5,600 cd/m2 at 16 V and the lowest turn on voltage of 4 V at 10 cd/m2. The EQE of OLEDs using these EMLs is relatively low, with a maximum value of ca. 5% at turn on. In addition, the EQE characteristics also displayed a strong roll-off at higher luminance values with devices having the intermolecular host TCTA:TPBi displaying the smallest decrease. The EQE roll-off is attributed to unbalanced injection and transport of holes and electrons in the EML. In all cases, the electroluminescence (EL) spectra resembles that of the emitter TBPe, having perhaps a different relative magnitude of the two EL peaks displayed by TBPe at ca. 460 nm and 495 nm. At this point, it is unclear why the EL of OLEDs having YZ-V-89:TBPe (97:3 & 94:6 vol.%) and 4CzDPO:TPBe(97:3 vol.%) EML display a maximum EL peak at 495 nm, while devices with a EML of TPBi:TCTA:TBPe (48:48:2 vol.%) display a stronger peak at 460 nm. As shown in Figure 17, after some optimization 4CzDPO:TPBe OLEDs showed an EL spectra and CIE values ca. (0.13, 0.25), that resembled those of OLED based on TBPe.

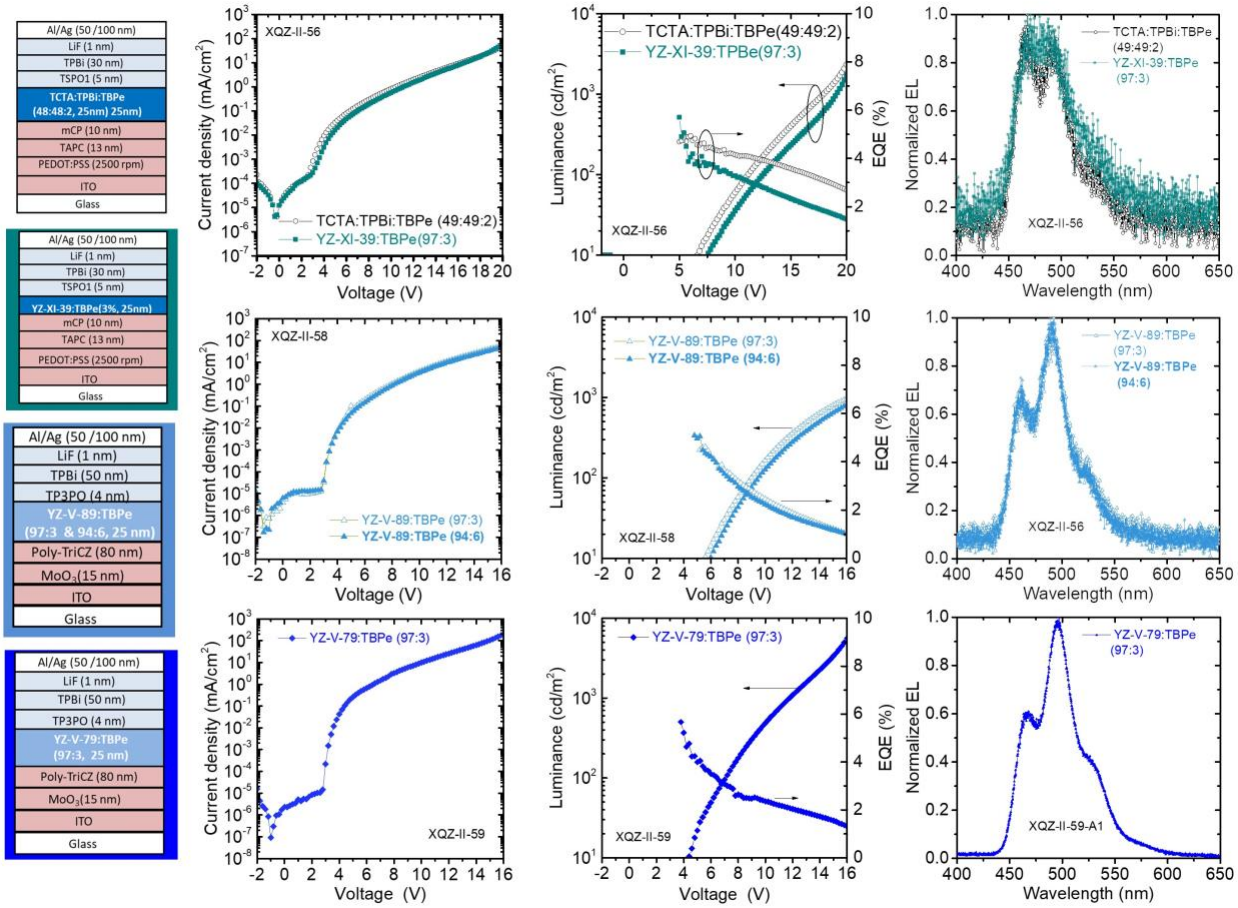

Figure 16. Device geometry (left column), current density vs. voltage and luminance vs. voltage characteristics (central columns) and electroluminescence spectra (right column) of OLEDs having 4 different emissive layers.

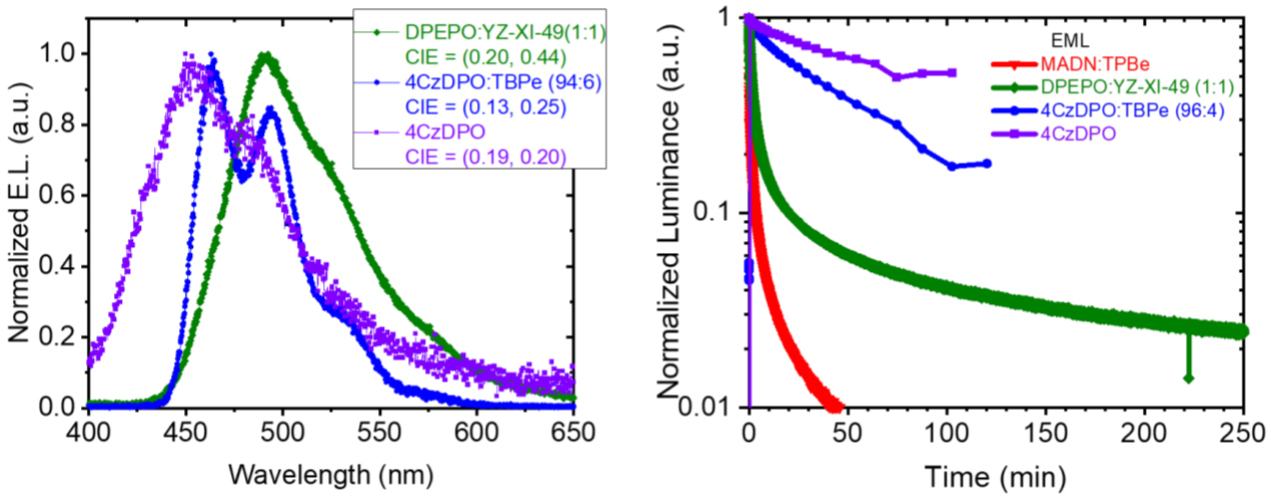

Figure 17. (left) Electroluminescence spectra (right) temporal dependent luminance of OLEDs having 4 different emissive layers.

Figure 17, shows a comparison of the EL spectra produced by OLEDs based on DPEPO:YZ-XI-49, 4CzDPO:TPBe and single-material 4CzDPO EMLs. This comparison revels the improvement in the CIE values achieved by the blue-OLEDs developed in this program. Although the efficiency of 4CzDPO-based OLED remains small when compared to that of DPEPO:YZ-XI-49 or YZ-XI-49 OLEDs[2], computational studies to be presented below reveal potential paths for optimization. However, it is worth pointing out that 4CzDPO-based OLED still outperform benchmark MADN:TBPe-based fluorescent OLEDs, yielding higher EQE values and 10×longer LT_{70} lifetime values, as shown in Figure 17. With respect to device lifetime measurements, it most be pointed out that the conditions of our evaporation system where not optimum device lifetimes due to the heavy material screening performed during this program. Hence, the evolution of the luminance reported in Figure 17 represent not the maximum lifetime values expected from these OLEDs, but a relative comparison between devices fabricated under roughly identical conditions. Consequently, while these results are preliminary, since significant statistics and optimization of the deposition conditions will be necessary to validate them, they are certainly very encouraging.

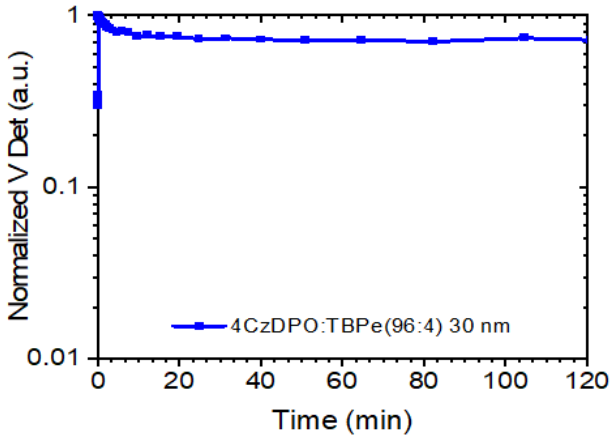

Figure 18. Photoluminescence lifetime of 4CzDPO:TPBe emissive layer.

Furthermore, Figure 18 shows the results of photoluminescence lifetime studies under continuous irradiation of a 300 nm UV LED (350 mW/cm$_2$) that suggest that the photostability of these intramolecular 4CzDPO:TPBe emissive layer is at least as good as that of TBPe. We also observed decreased photostability, more rapid degradation, on emissive layers comprising a host:TADF emitter and in single material TADF emitter having large ΔE_{ST} values (>200 meV); which seems to further support the validity of our initial hypothesis.

To rationalize efficient FRET observed and difficulties in device optimization, computational studies of the so-called hyperfluorescence in 4DCzPO:TBPe were also carried out.

The relative orientations of the TADF and fluorescent molecules can strongly influence the charge-transport, energy-transfer, and excitonic properties in an emissive thin film. Atomistic molecular dynamics (MD) simulations were performed to study the morphology of the EML. We calculated the radial distribution functions (RDFs), which describe the probability of finding a particle at a distance (r) from a reference particle. The centers-of-mass of the TBPe emitters (COM_{TBPe}) and acceptor subunit (A) of 4CzDPO (COM_A) were evaluated (Figure 19(a)) and the corresponding RDFs are shown in Figure 19(b) (black line). The oxadiazole (acceptor) moiety in 4DCzPO is found to be located too far away from the COM_{TBPe} (the corresponding RDF starts to have a non-zero value for r > 6.5 Å) to form any *inter*-molecular π–π stacking between these units. This is mainly because the *intra*-molecular conformation of 4DCzPO allows the four donor moieties to shield the oxadiazole segment from short-range *inter*-molecular interactions (Figure 19(c)). However, the donor subunits are available to interact with TBPe emitters. Figure 19(b) (red line) shows that the peak maximum of the RDF between the centers-of-mass of the donor subunits (D) of 4CzDPO (COM_D) and COM_{TBPe} is located at ca. 4.1 Å, which corresponds to short-range *inter*-molecular interactions via π–π stacking (Figure 19(c)). Furthermore, we note that the first RDF peak between the tertiary carbon of the tert-butyl substituents of TPBe and COM_D appears at 5.1 Å. This allows the methyl groups of the side-chains to interact with the donor segments of 4DCzPO via Van der Waals forces. It is also worth mentioning that this EML is simulated to display a glassy behavior which implies that the molecular motions of 4DCzPO are significantly restricted once the film is fabricated.

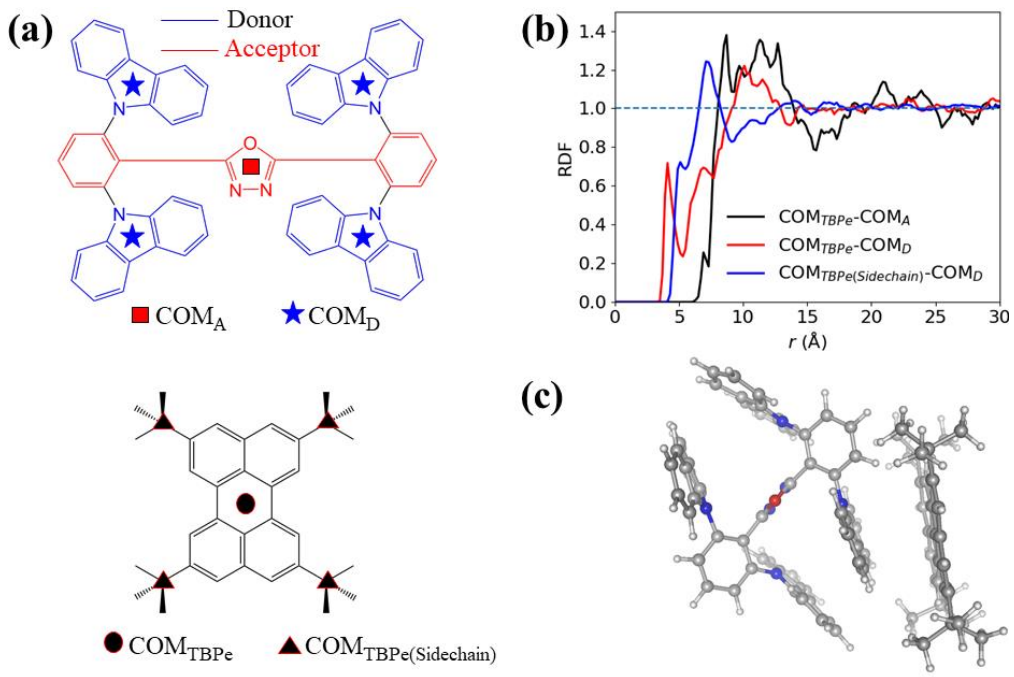

Figure 19. (a) Illustration of the centers-of-mass of acceptor and donor subunits of a 4CzDPO molecule (COM_A & COM_D), and the centers-of-mass of a TBPe emitter (COM_{TBPe}) and its sidechains ($COM_{TBPe(Sidechain)}$). (b) RDFs between COMs illustrated in (a). (c) Illustration of the π–π *inter*-molecular interactions between TBPe and a donor subunit of 4CzDPO.

The electronic structure of 4CzDPO and TBPe were calculated using long-range corrected density functional theory (DFT) at the ωPCMB97XD level, complemented by time-dependent DFT (TDDFT) calculations to characterize the nature of the 4CzPDO S_1 and T_1 states and the results found to produce good agreement with the photoluminescence data.

The ISC and RISC rates (k_{ISC} and k_{RISC}, respectively) for 4CzDPO where calculated using Marcus semiclassical electron-transfer theory. The distributions in spin–orbit couplings (V_{SOC}) and ΔE_{ST} for these 4CzDPO molecules yielded mean absolute values of 0.03 and 70 meV, respectively. Using the calculated V_{SOC} and ΔE_{ST} values along with the reorganization energy estimated for the intersystem crossing process, the mean values of k_{ISC} and k_{RISC} are estimated to be 1.10×10^7 s^{-1} and 9.06×10^5 s^{-1}, respectively. The radiative transition rate for 4CzDPO was found to be only about half of k_{ISC}; therefore, 4CzDPO is likely to undergo only a few cycling transitions between the S_1 and T_1 states before it radiatively decays to the ground state; explaining the relatively short lifetime for delayed fluorescence (4 μs) that we experimentally measured in 4CzDPO neat films.

The excitation energy transfer (EET) rates between 4CzDPO and TPBe molecules were evaluated. The electronic couplings for EET were estimated using an approach based on the electron transition densities derived from TDDFT calculations. The results of these calculations, shown in Figure 20, indicate that the Förster mechanism (FRET) is the dominant mechanism for energy transfer, and the short-range Dexter energy-transfer mechanism plays only a minimal role in the emissive layer of 4CzDPO:TPBe. Using the calculated electronic couplings, the rates for the singlet-exciton energy transfers SEET (k_{SEET}) process among the pairs extracted from the MD simulations were estimated. The values of energy transfer rate from 4CzDPO to TBPe can be as

high as 2.70 × 10^{11} s^{-1} and are four orders of magnitude larger than the values for the reverse process of energy transfer from TBPe to 4CzDPO (1.63 × 10^{7} s^{-1}).

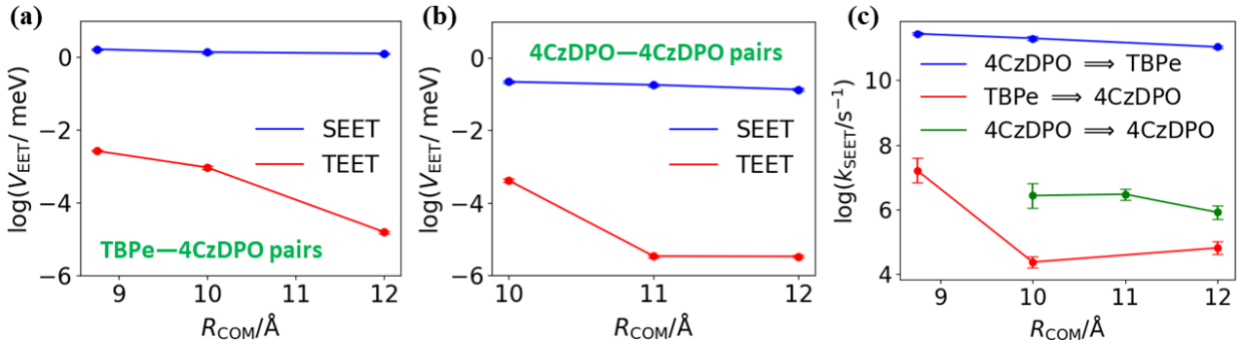

Figure 20. (a, b) Absolute electronic couplings of excitation-energy transfers for singlet (SEET) and triplet (TEET) excitons as a function of COM separation. (c) Calculated rates for SEET using the corresponding electronic couplings. The couplings and rates are estimated by considering 1,600 pairs extracted from the MD simulations.

The k_{SEET} values of energy transfer among 4CzDPO dimers (4CzDPO => 4CzDPO) are calculated to be 3.7 × 10^{6} s^{-1}, values almost comparable to the k_r (4.8 × 10^{6} s^{-1}) and k_{ISC} (1.1 × 10^{7} s^{-1}) values in 4CzDPO, but considerably smaller than the energy-transfer rates from 4CzDPO to TBPe (2.7 × 10^{11} s^{-1}). Although the difference in the electronic coupling, V_{SEET}, contributes to larger k_{SEET} values for transfer from 4CzDPO to TBPe than from 4CzDPO to 4CzDPO, the difference is mainly due to a much larger Franck-Condon factor for the 4CzDPO to TBPe energy transition than for the 4CzDPO to 4CzDPO transition. A direct consequence of these transitions rates is that, as soon as a singlet exciton is formed on 4CzDPO, the excitation transfers to TPBe. Since the TBPe excitons thus generated exhibit significantly larger k_r values than 4CzDPO excitons, the delayed fluorescence is accelerated and the overall fluorescence lifetime is reduced, in good agreement with our experimental measurements described above (2 μs for 4CzDPO:TBPe vs. 4 μs for 4CzDPO neat films).

We also found that the SEET rates among 4CzDPO molecules are comparable to the rates of radiative decay and intersystem crossing for the TADF molecules. Energy-transfer processes in 4CzDPO neat films can promote luminescence quenching via exciton–exciton annihilation or exciton decay at device interfaces, which ultimately decreases the photoluminescence quantum yields (PLQY). The PLQY can be expressed as:

$$\mathrm{PLQY} = \frac{k_r}{k_r + k_{ISC} + k_{SEET} + k_{nr}} \times 100 \qquad (1)$$

where, k_{nr} denotes the nonradiative recombination rate constant. Based on the Marcus-Levich-Jortner model,[7] the k_{nr} rates in 4CzDPO are estimated to be smaller than 1 × 10^{6} s^{-1}. Using the relation above, the PLQY is calculated to be 23%, which is in good agreement with the experimental PLQY value in 4CzDPO neat films, 17%.

Finally, it is worth pointing out that morphology analyses show that due to a D-A-D structural motif, the oxadiazoles are semi-buried by carbazole moieties, suppressing electron transport in the emissive layer, in good agreement with the results at the device level. These insights may therefore provide guidance for the design of novel molecules having balanced charge transport properties and for the optimization of devices.

Task 3.1 Tandem WOLEDs fabrication.

We incorporated best performing blue EML into tandem WOLED geometries.

Subtask 3.1.1 WOLED efficiency and CRI. We characterized and performed a preliminary optimization of WOLEDs. Work was redefined to be focused on the optimization of blue OLEDs.

Subtask 3.1.2 WOLED lifetime (lumen maintenance studies)

We conducted preliminary lumen maintenance studies on the best-performing blue OLEDs**.** Work was redefined to be focused on the optimization of blue OLEDs.

Highlights of results:

Using gen-1 and gen-2 intramolecular host, we fabricated tandem WOLEDs using single-material emissive layers to validate the approach. As the program moved forward, we found that challenges associated with the fabrication, characterization and optimization of blue OLEDs required to focus resources in order to produce significant breakthroughs in performance to justify spending time in fabricating WOLEDs. We believe that progress made during this program in the development of blue OLEDs can set a solid foundation for the development of WOLEDs that meet the ambitious metrics of this program.

Project Output

A. Publications/conferences

(1) X. Zhang, M. W. Cooper, Y. Zhang, C. Fuentes-Hernandez, S. Barlow, S. R. Marder, B. Kippelen, "Host-Free Yellow-Green Organic Light-Emitting Diodes with External Quantum Efficiency over 20% Based on a Compound Exhibiting Thermally Activated Delayed Fluorescence", ACS Appl. Mater. Interf., 2019, 11, 12693-12698 (doi: 10.1021/acsami.8b18798).

(2) X. Zhang, C. Fuentes-Hernandez, Y. Zhang, M. W. Cooper, S. Barlow, S. R. Marder, B. Kippelen, "High Performance Blue-Emitting Organic Light-Emitting Diodes from Thermally Activated Delayed Fluorescence: A Guest/Host Ratio Study", J. Appl. Phys., 2018, 124, 055501/055501-055507 (doi: 10.1063/1.5041447).

(3) M. W. Cooper, X. Zhang, Y. Zhang, S. O. Jeon, H. Lee, S. Kim, C. Fuentes-Hernandez, S. Barlow, B. Kippelen, S. R. Marder, "Effect of the Number and Substitution Pattern of Carbazole Donors on the Singlet and Triplet State Energies in a Series of Carbazole-Oxadiazole Derivatives Exhibiting Thermally Activated Delayed Fluorescence", Chem. Mater., 2018, 30, 6389-6399 (doi: 10.1021/acs.chemmater.8b02632).

(4) M. W. Cooper, X. Zhang, Y. Zhang, C. Fuentes-Hernandez, S. Barlow, B. Kippelen, S. R. Marder, "Control of Singlet Emission Energy in a Diphenyloxadiazole Containing Fluorophore Leading To Thermally Activated Delayed Fluorescence", ACS Omega, 2018, 3, 14918-14923 (doi: 10.1021/acsomega.8b01979).

(5) X.K. Chen, B.W. Bakr, M. Auffray, Y. Tsuchiya, C.D. Sherrill, C. Adachi, J.L. Bredas, Intramolecular Noncovalent Interactions Facilitate Thermally Activated Delayed Fluorescence (TADF), Journal of Physical Chemistry Letters, 10 (2019) 3260-3268.

(6) X.K. Chen, D. Kim, J.L. Bredas, Thermally Activated Delayed Fluorescence (TADF) Path toward Efficient Electroluminescence in Purely Organic Materials: Molecular Level Insight, Accounts of Chemical Research, 51 (2018) 2215-2224.

(7) H. Noda, X.K. Chen, H. Nakanotani, T. Hosokai, M. Miyajima, N. Notsuka, Y. Kashima, J.L. Bredas, C. Adachi, Critical role of intermediate electronic states for spin-flip processes in charge-transfer-type organic molecules with multiple donors and acceptors, Nature Materials, 18 (2019) 1084-1090.

(8) H. Abroshan, E. Cho, V. Coropceanu, and J. L. Brédas, Suppression of Concentration Quenching in Ortho-Substituted Thermally Activated Delayed Fluorescence Emitters, Advanced Theory and Simulations, (2019), accepted, DOI: 10.1002/adts.201900185.

(9) Fuentes-Hernandez, C., Jia, X., Zhang, Park, Y., X., Larrain, F.A., Kippelen, B. "Recent Advances in Organic Materials and Devices for Adaptive Solid-State Lightning." Presented at SPIE Optics and Photonics, San Diego, CA, August 20th, 2018

(10) Fuentes-Hernandez, C. "Stable White Organic Light Emitting Diodes Enabled by New Material with Reduced Excited-State Lifetimes." 2018 U.S. Department of Energy Solid-State Lightning R&D Workshop, Nashville, TN, January 30th, 2018

(11) B. Kippelen, "*Organic optoelectronics: the endless frontier*," 10th annual USA India Business Summit, 25th Annual Georgia Tech Global Business Forum, "Global Advanced Industries: Creating Local Opportunities," Aug. 27-28, Atlanta, GA (2019).

(13) B. Kippelen, C. Fuentes-Hernandez, X. Zhang, Y. Zhang, M. W. Cooper, S. Barlow, S. R. Marder, Z. Zheng, V. Coropceanu, J. L. Brédas, *"Recent advances in TADF materials and devices,"* Optical Probes 2019 Conference, Jul. 7-12, Vilnius, Lithuania, (2019).

(14) B. Kippelen, *"Organic photonics and electronics: the endless frontier,"* 3rd International Symposium on Molecular Design of Optoelectronic Materials, ICCAS, May 22-24, Beijing, China (2019).

(15) B. Kippelen, *"Organic optoelectronics rhapsody,"* presented at SPIE Security and Defense, Sep. 9-12, Strasbourg, France (2019).

(16) X. Zhang, C. Fuentes-Hernandez, Y. Zhang, M. W. Cooper, S. Barlow, S. R. Marder, and B. Kippelen, *"A reevaluation of emissive layer design for high performance blue-emitting organic light-emitting diodes from thermally activated delayed fluorescence,"* poster presented at the 2018 STAMI Industrial Partners Day and Exposition, Atlanta, GA, Sep. 27-28 (2018).

(17) S. Abraham, C. Fuentes-Hernandez, X. Jia, J. Inman, N. Hertel and B. Kippelen, *"Plastic scintillators based on polystyrene-TADF-Bismuth ternary systems for gamma spectroscopy,"* poster presented at the 2018 STAMI Industrial Partners Day and Exposition, Atlanta, GA, Sep. 27-28 (2018).

(18) B. Kippelen, *"Organic materials and devices for next-generation imaging applications,"* presented at SPIE Photonics West Conference, Feb. 3-7, San Francisco, CA (2019).

(19) B. Kippelen, C. Fuentes-Hernandez, X. Zhang, Y. Zhang, M. W. Cooper, S. Barlow, and S. R. Marder,*"Recent advances in organic light-emitting diodes based on thermally activated delayed fluorescence,"* International Conference on

Electroluminescence and Optoelectronic Devices (ICEL), Jeju Island, Korea, Oct. 14-17 (2018).

References:

1. Lee, D. R.; Choi, J. M.; Lee, C. W.; Lee, J. Y., Ideal Molecular Design of Blue Thermally Activated Delayed Fluorescent Emitter for High Efficiency, Small Singlet–Triplet Energy Splitting, Low Efficiency Roll-Off, and Long Lifetime. *ACS Appl. Mater. Inter.* **2016,** *8* (35), 23190-23196.
2. Zhang, X.; Fuentes-Hernandez, C.; Zhang, Y.; Cooper, M. W.; Barlow, S.; Marder, S. R.; Kippelen, B., High performance blue-emitting organic light-emitting diodes from thermally activated delayed fluorescence: A guest/host ratio study. *J. Appl. Phys.* **2018,** *124* (5), 055501.
3. Zhang, X.; Cooper, M. W.; Zhang, Y.; Fuentes-Hernandez, C.; Barlow, S.; Marder, S. R.; Kippelen, B., Host-Free Yellow-Green Organic Light-Emitting Diodes with External Quantum Efficiency over 20% Based on a Compound Exhibiting Thermally Activated Delayed Fluorescence. *ACS Appl. Mater. Inter.* **2019,** *11* (13), 12693-12698.
4. Abroshan, H.; Cho, E.; Coropceanu, V.; Brédas, J.-L., Suppression of Concentration Quenching in Ortho-Substituted Thermally Activated Delayed Fluorescence Emitters. *Advanced Theory and Simulations* **2020,** *3* (2), 1900185.
5. Cooper, M. W.; Zhang, X.; Zhang, Y.; Jeon, S. O.; Lee, H.; Kim, S.; Fuentes-Hernandez, C.; Barlow, S.; Kippelen, B.; Marder, S. R., Effect of the Number and Substitution Pattern of Carbazole Donors on the Singlet and Triplet State Energies in a Series of Carbazole-Oxadiazole Derivatives Exhibiting Thermally Activated Delayed Fluorescence. *Chem. Mat.* **2018,** *30* (18), 6389-6399.
6. Cooper, M. W.; Zhang, X.; Zhang, Y.; Fuentes-Hernandez, C.; Barlow, S.; Kippelen, B.; Marder, S. R., Control of Singlet Emission Energy in a Diphenyloxadiazole Containing Fluorophore Leading To Thermally Activated Delayed Fluorescence. *ACS Omega* **2018,** *3* (11), 14918-14923.
7. Jortner, J., Temperature-Dependent Activation-Energy for Electron-Transfer between Biological Molecules. *J Chem Phys* **1976,** *64* (12), 4860-4867.